Atmos. Chem. Phys. Discuss., 12, 20483–20517, 2012
www.atmos-chem-phys-discuss.net/12/20483/2012/
doi:10.5194/acpd-12-20483-2012

Atmospheric Chemistry and Physics Discussions

Droplet number prediction uncertainties from CCN: an integrated assessment using observations and a global adjoint model

R. H. Moore[1,*], **V. A. Karydis**[2], **S. L. Capps**[1], **T. L. Lathem**[2], **and A. Nenes**[1,2]

[1]School of Chemical & Biomolecular Engineering, Georgia Institute of Technology, Atlanta, Georgia, USA
[2]School of Earth & Atmospheric Sciences, Georgia Institute of Technology, Atlanta, Georgia, USA
[*]now at: NASA Postdoctoral Program, NASA Langley Research Center, Hampton, Virginia, USA

Received: 29 June 2012 – Accepted: 9 August 2012 – Published: 16 August 2012

Correspondence to: A. Nenes (athanasios.nenes@gatech.edu)

Published by Copernicus Publications on behalf of the European Geosciences Union.

Abstract

We use the Global Modeling Initiative (GMI) chemical transport model with a cloud droplet parameterization adjoint to quantify the sensitivity of cloud droplet number concentration to uncertainties in predicting CCN concentrations. Published CCN closure prediction uncertainties for six different sets of simplifying compositional and mixing state assumptions are used as proxies for modeled CCN uncertainty arising from application of those scenarios. It is found that cloud droplet number concentrations are fairly insensitive to CCN-active aerosol number concentrations over the continents ($\partial N_d/\partial N_a \sim 10$–$30\,\%$), but the sensitivities exceed 70 % in pristine regions such as the Alaskan Arctic and remote oceans. Since most of the anthropogenic indirect forcing is concentrated over the continents, this work shows that the application of Köhler theory and attendant simplifying assumptions in models is not a major source of uncertainty in predicting cloud droplet number or anthropogenic aerosol indirect forcing for the liquid, stratiform clouds simulated in these models. However, it does highlight the sensitivity of some remote areas to pollution brought into the region via long-range transport (e.g. biomass burning) or from seasonal biogenic sources (e.g. phytoplankton as a source of dimethylsulfide in the southern oceans). Since these transient processes are not captured well by the climatological emissions inventories employed by current large-scale models, the uncertainties in aerosol-cloud interactions during these events could be much larger than those uncovered here. This finding motivates additional measurements in these pristine regions, which have recieved little attention to date, in order to quantify the impact of, and uncertainty associated with, transient processes in effecting changes in cloud properties.

1 Introduction

The ability of atmospheric aerosols to act as cloud condensation nuclei (CCN) remains one of the largest sources of uncertainty in current global climate modeling

ACPD
12, 20483–20517, 2012

efforts (Solomon et al., 2007). This is because aerosols are chemically-complex and are derived from a variety of primary emissions sources as well as secondary gas-to-particle conversion in the atmosphere. Given this complexity, there is a need for an extensive global observational dataset that can be used to improve the representation of aerosol-cloud interactions in models.

Measurements of CCN spectra (i.e. CCN concentrations over a range of water vapor supersaturations) have been made for decades (e.g. Twomey, 1977; Hudson, 1993, and references therein) and have yielded CCN datasets at a number of locations worldwide. While providing information on the spatiotemporal variation of CCN concentrations and the total particle size distributions, many of these pioneering studies lacked the detailed aerosol composition information needed to fully explain the observed CCN variability. Recent improvements in instrument capabilities have greatly improved the state of the art for measuring the chemical composition and CCN activity of aerosols. This includes the development of the Particle-Into-Liquid Sampler (PILS, Weber et al., 2001) for measuring water-soluble aerosol composition, the Aerodyne Aerosol Mass Spectrometer (AMS, Jayne et al., 2000; Jimenez et al., 2003) for measuring non-refractory aerosol composition, and the Droplet Measurement Technologies Continuous-Flow, Streamwise, Thermal-Gradient CCN Counter (CCNC, Roberts and Nenes, 2005; Lance et al., 2006) for measuring CCN activation and droplet growth. Together with traditional and newer techniques for measuring the aerosol size distribution (e.g. Wang and Flagan, 1989; Flagan, 2004; Cai et al., 2008; Olfert et al., 2008), these robust and commercially-available instruments have enabled a multitude of field studies that have comprehensively characterized the compositional and size dependence of ambient CCN. With this information, it is now possible to empirically evaluate our theoretical understanding of aerosol-cloud interactions using in situ field data.

CCN concentrations are almost exclusively predicted in models with Köhler theory (Köhler, 1936), which has been shown to adequately capture the CCN activity of single- and multi-component aerosol by a large number of laboratory studies (e.g. Cruz and Pandis, 1997; Raymond and Pandis, 2002, 2003; Giebl et al., 2002; Padró et al., 2007).

ACPD
12, 20483–20517, 2012

However, atmospheric aerosols are often much more complex than those created in the laboratory, so application of Köhler theory-based models and parameterizations must necessarily make simplifying assumptions regarding the aerosol mixing state and composition in order to reduce their computational burden. To evaluate the uncertainty associated with these simplifying assumptions, a number of "CCN closure" studies have been performed, where the aerosol size distributions and chemical compositions measured in the field are used with the simplifying assumption scenarios to predict CCN number concentrations (N_{CCN}), which are then compared to concurrent CCN measurements with a CCNC. The deviation between the measured and predicted concentrations is interpreted as the uncertainty introduced by that set of simplifying assumptions.

While quantifying the uncertainty in our predictive understanding of CCN concentrations is important, it represents only one link in our understanding of the aerosol-cloud indirect effects on climate. The second link is the combination of CCN concentrations with cloud dynamics (e.g. ambient liquid water content, updraft velocity, and droplet condensational growth rates) to determine the overall cloud droplet concentration (N_d), which, in turn, affects the cloud albedo (A) and radiative properties. A few studies have combined ambient measurements of N_d with cloud parcel model simulations using measured N_{CCN} and dynamical parameters to perform "cloud droplet closure" (e.g. Hallberg et al., 1997; Chuang et al., 2000; Snider and Brenguier, 2000; Snider et al., 2003; Conant et al., 2004; Meskhidze et al., 2005; Fountoukis et al., 2007). The agreement between predictions and measurements has generally been quite good despite large observed aerosol variability in some studies, with average N_d predicted-to-measured ratios on the order of 0.71–1.2 and some larger ratios reported by Hallberg et al. (1997).

In addition to these field studies, model simulations are an important tool for examining the sensitivity of N_d to changes in CCN and other parameters by selectively turning on and off certain effects. For example, Lance et al. (2004) used a large number of 1-D parcel model simulations to look at the competing influences of aerosol chemistry and cloud updraft velocity in determining N_d under a wide variety of conditions. They

ACPD
12, 20483–20517, 2012

found that chemical effects can account for 28–100 % of the variability in N_d for both marine and continental environments. Rissman et al. (2004) extended the droplet parameterization of Abdul-Razzak et al. (1998) to include the effects of surfactants and derived the analytical sensitivities of N_d with respect to the parameterization inputs, and reached a similar conclusion that N_d can be up to 1.5-times as sensitive to aerosol composition and surface tension effects as it is to cloud dynamical effects under certain atmospherically-relevant conditions. Sotiropoulou et al. (2006) used a droplet parameterization to propagate the CCN closure uncertainties observed by Medina et al. (2007) during the ICARTT campaign to uncertainties in N_d. Using a campaign-average, prescribed CCN spectrum and size distribution in the parameterization, they found the uncertainty of N_d to be 50 % of that for N_{CCN} over a range of conditions. Ervens et al. (2010) also modeled the sensitivity of N_d uncertainty to N_{CCN} uncertainty and found that a 100 % overprediction of N_{CCN} leads to only a 15 % overprediction in N_d. These findings highlight the influence of aerosols versus cloud dynamics, and motivate future work with larger scale, global models to better understand where clouds are most sensitive to aerosol composition effects and where they are not.

Toward this end, Sotiropoulou et al. (2007) parameterized the CCN uncertainty from the ICARTT study in terms of supersaturation and used this relationship with the global N_d and N_{CCN} outputs from the NASA Goddard Institute for Space Studies Version II' (GISS II') general circulation model (GCM) to quantify the resulting errors in N_d, aerosol indirect forcing, and autoconversion rate. This is achieved by running two present-day simulations: a base case simulation with normal present day emissions and a perturbed case simulation where the size distribution is varied to alter the CCN concentration according to the ICARTT uncertainty. Their results suggest that a global average CCN prediction error of 10–20 % translates into a 7–14 % uncertainty in N_d and a 10–20 % uncertainty in aerosol indirect forcing (Sotiropoulou et al., 2007). While this study gives important first-order constraints on how CCN uncertainty may affect global indirect forcing estimates, the approach does not account for regional differences in the uncertainty of N_{CCN} or how the model pertubation may induce other, non-linear effects in the sim-

ACPD
12, 20483–20517, 2012

ulation. A thorough discussion of some of these challenges is presented by Lee et al. (2011), who has developed a new statistical method for estimating model sensitivities to input uncertainies.

In summary, while there have been several studies to date examining the sensitivity of cloud droplet number concentration uncertainty to uncertainties in CCN number concentration, there is still no clear estimate of the global magnitude of this uncertainty or how it varies regionally. In this study, we address these questions by combining data obtained from over thirty-five published CCN closure studies with simulations conducted with the adjoint of the Kumar et al. (2009) cloud droplet parameterization, recently developed by Karydis et al. (2012). The adjoint tracks the sensitivity of model parameters to inputs concurrently with the forward model execution and without perturbing the simulation parameters. Thus, it is able to calculate the sensitivity of N_d to aerosol number concentration, N_a, or a large number of other parameters with analytical precision and requires only a single model run. In the following sections, we briefly discuss the published datasets and the adjoint model before comparing and contrasting the simulation results with observations. The goal of this work is to improve the understanding of the global and regional sensitivities of modeled cloud droplet number to the CCN concentration uncertainty introduced through simplified model assumptions regarding aerosol mixing state and chemical composition. This will inform both future planning of field measurement studies focused on CCN, as well as efforts to quantify model uncertainty and variability.

2 Methods

2.1 CCN prediction uncertainty measurements

In this work, we use CCN prediction uncertainties measured at multiple locations worldwide as a proxy for CCN prediction uncertainty in models employing Köhler theory. Table 1 lists the thirty-six closure study regions considered, which were selected because

ACPD
12, 20483–20517, 2012

they involve ambient measurements of CCN concentration, aerosol size distribution, and aerosol chemical composition. Additionally, each reports CCN closure uncertainties for at least one of six common closure scenarios as follows:

1. *Ammonium Sulfate:* all particles are composed of ammonium sulfate, with a prescribed Petters and Kreidenweis (2007) hygroscopicity parameter, κ, of 0.6 employed in the Köhler theory calculations.

2. *Internal Mixture, Soluble Organics:* all particles have the same composition as determined by the size-averaged, aerosol composition measurements. Organics are treated as soluble in Köhler theory with a prescribed κ of 0.11, which corresponds to a fully-soluble organic species with, e.g. a molar mass of 0.200 $\mathrm{kg\,mol^{-1}}$ and density of 1400 $\mathrm{kg\,m^{-3}}$.

3. *Internal Mixture, Insoluble Organics:* all particles have the same composition as determined by the size-averaged, aerosol composition measurements. Organics are treated as insoluble with $\kappa = 0$.

4. *External Mixture, Soluble Organics:* particles are composed of pure components (e.g. organic particles, ammonium sulfate particles, etc.), and the number of each type is determined by the size-averaged, aerosol composition measurements. Organics are treated as soluble with $\kappa = 0.11$.

5. *External Mixture, Insoluble Organics:* particles are composed of pure components (e.g. organic particles, ammonium sulfate particles, etc.), and the number of each type is determined by the size-averaged, aerosol composition measurements. Organics are treated as insoluble with $\kappa = 0$.

6. *Internal Mixture, Size-Dependent Composition, Insoluble Organics:* particles in each size distribution bin have the same composition as determined by the size-resolved, aerosol composition measurements, but the particle compositions in different size bins may vary. Organics are treated as insoluble with $\kappa = 0$.

ACPD
12, 20483–20517, 2012

These simplified mixing state and composition assumptions are characteristic of those used in large-scale models to improve computational efficiency. In another form of CCN closure, some other studies in the literature use the aerosol hygroscopicity obtained from humidified aerosol growth factor measurements to predict CCN concentrations with typically good agreement (e.g. Kim et al., 2011; Kammermann et al., 2010; Vestin et al., 2007; Good et al., 2010; Gasparini et al., 2006; Dusek et al., 2003; Covert et al., 1998, and others). While important for assessing the uncertainties associated with using the same hygroscopicity to predict both subsaturated and supersaturated water uptake, this type of closure study is not included here as it is less relevant for comparing against mass-composition-based models.

The studies shown in Table 1 reflect a diverse mixture of urban, rural, and marine sampling on both airborne and ground-based platforms. The majority of published studies focus on locations in North America, and CCN concentrations range from zero to a few thousand particles per cm^3 with the highest concentrations observed in the vicinity of local urban emissions sources (e.g. Houston, TX; Riverside, CA; Mexico City, Mexico) and within targeted biomass burning and ship plumes. Most studies report CCN concentration and closure data at a single or a few discrete supersaturations, and the tabulated values reflect the average across all supersaturations. A detailed description of each closure study location, measurements, and data analysis is given by the references in Table 1.

The CCN prediction uncertainties reported by these studies are shown in Table 2. Most studies tend toward overprediction with the external mixing scenarios producing lower predicted CCN concentrations than the ammonium sulfate or internal mixing scenarios. As discussed by Ervens et al. (2010), some studies report large CCN overpredictions on the order of 2–5-fold, which likely reflects the contribution of local emissions sources near the sampling locations that may produce a size-varying, externally-mixed aerosol that cannot be captured well from bulk chemical composition measurements. In some locations (e.g. Houston, TX, and Los Angeles, CA), airborne studies covering a wide horizontal and vertical sampling area report a smaller closure uncertainty than

ACPD
12, 20483–20517, 2012

that from ground-based sites in the same area. These conflicting values probably stem from the more local nature of the ground measurements versus the regional nature of airborne measurements. To capture the observed range of variablity, we evaluate the uncertainties from both sets of measurements, recognizing that the former are probably more relevant for finer-scale air quality modeling while the latter are probably more appropriate for comparison with coarser-resolution GCM climate predictions.

2.2 Model description

Simulations were conducted with the NASA Global Modeling Initiative (GMI; http://gmi.gsfc.nasa.gov) chemical transport model (CTM) using offline wind fields and an online aerosol simulation module coupled with the Kumar et al. (2009) droplet activation parameterization and its adjoint (Karydis et al., 2012). The GMI model is a modular CTM capable of multi-year, global simulations of aerosol concentrations and compositions (Rotman et al., 2001; Considine et al., 2005). The aerosol module used for this study is that of Liu et al. (2005), which uses emissions inputs for SO_2, dimethyl sulfide, elemental carbon (EC), organic carbon (OC), mineral dust, and sea salt; H_2O_2 is a chemical (secondary) species input from Liu et al. (2005). The online aerosol module outputs the global distribution of aerosol mass concentrations, which is used to drive the cloud droplet parameterization and its adjoint.

Before running the offline parameterization, the aerosol mass is first classified as one of four, externally-mixed aerosol modes: fossil fuels (SO_4^{2-}, OC, and EC), biomass burning (OC and EC), marine (SO_4^{2-} and sea salt), and mineral dust. The aerosol within each mode is assumed to be internally mixed and follow a prescribed size distribution as given by Chuang et al. (1997) and Radke et al. (1988) for fossil fuel aerosols, Anderson et al. (1996) for biomass burning aerosols, Lance et al. (2004) for marine aerosols, and d'Almeida (1987) for mineral dust aerosols. The aerosol number concentration for each type is then computed using these size distributions and a mass-fraction-weighted

ACPD
12, 20483–20517, 2012

average of the component densities (e.g. SO_4^{2-}, OC, EC) as described in more detail by Karydis et al. (2011).

The aerosol number distributions are then used to drive, offline, a cloud droplet parameterization (Kumar et al., 2009; Barahona and Nenes, 2007; Fountoukis and Nenes, 2005; Nenes and Seinfeld, 2003) that employs a physically-based method for calculating the aerosol CCN spectrum (i.e. the number of particles that act as CCN as a function of supersaturation) and the maximum supersaturation, s_{max}, for ascending cloud parcels in the global model. The total cloud droplet number, N_d, is then the value of the CCN spectrum at s_{max} in each model grid cell. Recently, the adjoint of the cloud droplet parameterization has been developed (Karydis et al., 2012), which calculates the sensitivity of N_d to the parameterization input parameters (i.e. aerosol concentration and composition) during the forward model run. This allows the simultaneous computation of both the mean parameter values and their sensitivities with analytical precision.

2.3 Model application

The model simulation represents a single, climatological year (in this case from March 1997 to February 1998), including a one-month spin up time that is not included in the analysis. This simulated time period was selected to complement the modeling study of Karydis et al. (2011). Meteorological fields were obtained from the GISS II' global climate model (Koch and Rind, 1998; Rind and Lerner, 1996), with a horizontal resolution of 4° latitude by 5° longitude and with 23 vertical layers from surface pressure to 0.01 hPa. The meteorological information in the simulation was updated every three hours. For the droplet parameterization and its adjoint, a constant effective water uptake coefficient of 0.06 was assumed (Fountoukis et al., 2007), and realistic updraft velocities were prescribed based on observed values for stratocumulus clouds over land ($w = 0.3\,m\,s^{-1}$) and ocean ($w = 0.15\,m\,s^{-1}$) (Chuang et al., 2000; Guibert et al.,

ACPD
12, 20483–20517, 2012

2003; Meskhidze et al., 2005). The model simulations have been previously evaluated against observations by Karydis et al. (2011) with reasonably good agreement.

3 Results and discussion

3.1 Global aerosol concentration (N_a) distributions

The simulated global annual mean aerosol concentration, N_a, is shown in Fig. 1a and is found to be mostly anti-correlated with s_{max} over the continents (not shown), consistent with the mechanism of increased CCN concentrations in modulating cloud dynamics (i.e. aerosol indirect effects). The highest concentrations (and lowest s_{max}) are seen over the Eastern United States, Europe, and East Asia from anthropogenic emissions. Higher concentrations are also predicted for the Southern Hemisphere near and downwind of biomass burning sources. Meanwhile, the lowest concentrations (and highest s_{max} occur in the pristine southern and subtropical oceans and the Alaskan-Canadian Arctic. The simulated global geometric mean aerosol concentration is $502^{\times}_{\div}5.52$ for a mean s_{max} of $(0.07 \pm 0.03)\%$.

A quantitative comparison between the simulated N_a and N_d at s_{max} and the observed N_{CCN} at varying supersaturation is given in Table 3. While the s_{max} in these locations is similar to the global average, the simulated N_a and N_d are much higher than the global average due to the past focus on conducting closure studies over the continents. For many regions, simulated concentrations agree reasonably well with the observed range of values, although much higher simulated to observed concentration ratios are found in a number of locations (e.g. the Amazon Rainforest, Duke Forest, Finokalia, the Florida coast, the Gulf of Mexico, Jeju Island, and others), which may be reflective of seasonal differences or varying local emissions sources that are not captured by either the short-term field study or the simulated annual mean.

ACPD
12, 20483–20517, 2012

3.2 Global cloud droplet concentration (N_d) distribution and relative sensitivity of N_d to N_a

Simulated droplet concentrations, N_d, are also shown in Table 3 and in Fig. 1b. The global distribution of N_d is similar to that of N_a but with substantially lower concentrations (approximately five-fold on average). This is shown quantitatively in Fig. 2, where it can been seen that 50–100 % of aerosol form droplets at low concentrations, but the impact on N_d of increasing N_a gradually decreases above $\sim 100\,cm^{-3}$. This implies that the sensitivity of N_d to aerosol depends on the activation fraction, which, in turn, is governed by N_a and s_{max} through the CCN spectrum. Low values of N_a correlate with the highest s_{max} and greatest cloud droplet sensitivity, while the highest N_a correlate with the lowest s_{max} and smallest cloud droplet sensitivity. The sensitivity decreases from 80–90 % at $100\,cm^{-3}$ to nearly zero at 10^4–$10^5\,cm^{-3}$; however, there is no clear trend in s_{max} within this transition region (Fig. 2). This transition arises as aerosol concentration effects become more important than cloud dynamics in determining N_d, and occurs around the inflection point of the sigmoidal fit function ($N_a \sim 400\,cm^{-3}$).

As discussed by Karydis et al. (2012), the coarse mode of sea salt aerosol in the model can act as giant CCN (GCCN) in some regions (e.g. the North Atlantic Ocean). GCCN are large enough to activate at very low supersaturations and remove enough water vapor through their condensational growth that the local cloud s_{max} is decreased. This means that fewer droplets form, resulting in an inverse-Twomey effect and potentially a reduction in shortwave cloud forcing (i.e. $\partial N_d/\partial N_a < 0$). It is difficult to constrain the variability of GCCN, but they likely comprise a negligible fraction of overall measured in situ CCN concentrations. Consequently, for this study, we fix the sea salt partial N_d sensitivity to values greater than or equal to zero (i.e. $\partial N_d/\partial N_{a,seasalt} \geq 0$), noting that the sensitivity may actually become negative in areas with close-to-zero sensitivities in Fig. 1.

The N_d sensitivities shown in Table 3 indicate that most of the closure studies carried out in the past decade have taken place in moderately to heavily-polluted areas, where

ACPD
12, 20483–20517, 2012

N_d is weakly sensitive to changes in N_a (~ 10–30 %). Two studies in the Alaskan and Canadian Arctic show lower simulated N_a and higher simulated s_{max} and sensitivity of N_d to N_a (~70 %). The global mean sensitivity is 0.46 ± 0.22.

Sotiropoulou et al. (2007) simulated global cloud droplet number concentrations and anthropogenic aerosol indirect forcing using the GISS II' GCM and uncovered a similar global mean droplet concentration and geographical distribution as modeled here, but with nearly two-fold lower droplet concentrations in some continental regions. As expected, the spatial pattern of regional aerosol indirect forcing corresponded to the spatial pattern of N_d. Thus, we expect the results of this study to be directly relevant for aerosol indirect forcing estimates even though the direct calculation of aerosol indirect forcing with a radiative transfer model is not performed here.

3.3 Global cloud albedo (*A*) distribution and relative sensitivity of *A* to N_a

The cloud droplet sensitivity discussed in the previous section provides important information regarding the potential sensitivity of clouds in a given region to changes in aerosol concentrations, but it says nothing about whether or not the clouds would form in the first place. This is because global and regional cloudiness is driven by dynamics (e.g. vertical updrafts) and moisture fluxes (e.g. liquid water content) in addition to the presence of CCN. Quantifying these individual processes on a global scale is challenging; however, satellite measurements over the past decades have been able to discern global cloudiness with good accuracy. In this study, we use the global annually-averaged cloud albedo (A) obtained from the NASA CERES mission to capture all of these effects. The cloud albedo is found by differencing the total sky and clear sky albedos for 2003 obtained from the NASA Giovanni online data system (Acker and Leptoukh, 2007). The global mean cloud albedo is 0.14 out of a mean total sky planetary albedo of 0.29. Since A incorporates both cloudiness fraction and the reflectivity of those clouds, it directly captures the indirect effect of aerosols on clouds. The global distribution of A is shown in Fig. 3a. Synoptic scale dynamics play a large role in the observed distribution of A, with higher albedos seen along the equatorial intertropi-

ACPD
12, 20483–20517, 2012

cal convergence zone (ITCZ) and in the mid-latitudes. Meanwhile, the observed cloud albedo is lowest in the subtropical subsidence zones.

In a landmark paper, Twomey (1991) defined the cloud albedo susceptibility to cloud droplet number as

$$\frac{\partial A}{\partial N_d} = \frac{A(1-A)}{3N_d} \quad (1)$$

for a constant amount of liquid water and by making a number of simplifying assumptions regarding the radiative properties of liquid water droplets. Equation (1) indicates that A is at peak sensitivity to N_d when $A = 0.5$, where $\partial A/\partial N_d = \frac{1}{12}N_d$.

Combining $\partial A/\partial N_d$ obtained from the CERES satellite measurements and Eq. (1) with $\partial N_d/\partial N_a$ obtained from the GMI model simulations yields the overall sensitivity of cloud albedo to aerosol concentration, $\partial A/\partial N_a$, which is shown in Fig. 3b. Overall, the spatial distribution of the albedo sensitivity is very similar to the cloud droplet number sensitivity, except that the former exhibits decreased sensitivity in the subtropical subsidence zones, where both N_d and cloudiness are low. The most sensitive regions are in the southern oceans and Arctic regions where a doubling of aerosol concentrations can be seen to induce a 20–30 % relative change in albedo. However, it is important to note that the sensitivities presented here do not include the mitigating effects of dynamical feedbacks (e.g. Koren and Feingold, 2011; Stevens and Feingold, 2009). Consequently, while the magnitude of this sensitivity may reflect an upper limit, the spatial distribution shown in Fig. 3b shows the key regions of the world where the sensitivity of cloud properties to aerosol is large.

3.4 Cloud droplet number uncertainties and implications for the indirect effect

In this section, the CCN closure uncertainties from Sect. 2.1 (Table 2) and the modeled cloud droplet sensitivities from Sect. 3.2 (Table 3) are combined to estimate the overall N_d uncertainty arising from the application of simplified forms of Köhler theory typically applied in global modeling studies of aerosol-cloud interactions. Figure 4

ACPD
12, 20483–20517, 2012

gives the field measurement uncertainties for five of the six closure scenarios. The left panels show the approximate spatial extent of those study areas located in North America and Europe and are colored by the N_{CCN} overprediction uncertainty $\left(\frac{\Delta N_{CCN}}{N_{CCN}}\right)$ from Table 2. The right panels show the estimated N_d overprediction uncertainty $\left(\frac{\Delta N_d}{N_d}\right)$ calculated as $\frac{\Delta N_d}{N_d} = \left(\frac{\partial N_d}{\partial N_a}\right)\left(\frac{N_a}{N_d}\right)\left(\frac{\Delta N_{CCN}}{N_{CCN}}\right)$. The color scale for $\frac{\Delta N_{CCN}}{N_{CCN}}$ in Fig. 4 is twice that for $\frac{\Delta N_d}{N_d}$, with light blue denoting zero overprediction uncertainty (i.e. perfect agreement between Köhler theory predictions and measurements). For most regions in the continental United States and Europe, $\frac{\Delta N_d}{N_d}$ is quite small ($\sim$ 0–20 %), despite large $\frac{\Delta N_{CCN}}{N_{CCN}}$, which reflects the relative insensitivity of N_d to aerosol concentration uncovered by the model for continental regions (Fig. 1c). Larger $\frac{\Delta N_d}{N_d}$ values are observed in California, in the Alaskan and Canadian Arctic, and in the Amazon rainforest, although only one closure scenario is considered in the Amazon study. In Los Angeles, the large $\frac{\Delta N_d}{N_d}$ reflects the large (nearly five-fold) CCN overprediction uncertainty reported by Cubison et al. (2008) and Ervens et al. (2010) for all closure scenarios. In the Los Angeles basin and California Central Valley, Moore et al. (2012a) report smaller values of $\frac{\Delta N_{CCN}}{N_{CCN}}$ that vary from −59 to 79 %, and which translate into $\frac{\Delta N_d}{N_d} \sim -10$–20 %. Reported Arctic CCN uncertainties are considerably lower (Moore et al., 2011), but still have a large effect on $\frac{\Delta N_d}{N_d}$ because of the relatively low modeled droplet concentrations and relatively high modeled N_d sensitivities in pristine regions.

Table 4 shows average uncertainty statistics for the six closure scenarios in this study. These mean values reflect the bias of past closure studies toward locations within the North American continent, which limits the generalizability of these numbers to a global scale. Additionally, the number of studies and the locations of those studies employing each closure scenario are different, which prevents direct cross-scenario comparison. However, the ratio of $\left(\frac{\Delta N_d}{\Delta N_{CCN}}\right)\left(\frac{N_{CCN}}{N_d}\right)$ should be representative

ACPD
12, 20483–20517, 2012

of the domain-averaged sensitivities, which can be directly compared despite different sample sizes. We find this ratio to be fairly invariant at 0.29–0.37 for $\frac{\Delta N_d}{N_d} \sim 1$–23 %. The N_d uncertainty is consistent with the estimates of the N_d sensitivity made by Ervens et al. (2010) (∼15 %) using a parcel model and with average N_d uncertainties of 7–14 % reported by Sotiropoulou et al. (2007) for the United States and Europe. Interestingly, the average N_{CCN} uncertainties reported in the GCM study were also ∼ 10–20 %, suggesting a much larger N_d sensitivity than we find here (i.e. $\left(\frac{\Delta N_d}{\Delta N_{CCN}}\right)\left(\frac{N_{CCN}}{N_d}\right) \sim 0.7$ versus the 0.29–0.37 found in this study).

Sotiropoulou et al. (2007) also used the radiative transfer model embedded in the GISS II' GCM to express CCN prediction uncertainty in terms of cloud forcing. They find that a 10–20 % uncertainty in global N_{CCN} results in a 0.1–0.2 $W m^{-2}$ shortwave cloud forcing uncertainty, which is 10–20 % of the anthropogenic indirect effect predicted in the model to be $-1.00\,W m^{-2}$. While this uncertainty is relatively small on a global scale, regional effects are likely to be more substantial. This is especially true when considering larger CCN prediction uncertainties than the range of 10–20 % assumed by Sotiropoulou et al. (2007), and which are suggested by some regional CCN closure studies in Table 2.

4 Summary and conclusions

Modeling simulations conducted with the GMI chemical transport model and cloud parameterization adjoint are used to interpret and extend the results of thirty-six published CCN closure studies in the literature to estimate the overall uncertainty in cloud droplet number concentration from applying Köhler theory-based parameterizations with simplifying assumptions. We find that the prediction of cloud droplet number is most susceptible to CCN uncertainty at low aerosol concentrations ($N_a < 100\,cm^{-3}$) and becomes insensitive to uncertainty in N_{CCN} for concentrations above $10^4\,cm^{-3}$. Thus, pristine areas such as the Arctic and remote oceans are found to be most sen-

ACPD
12, 20483–20517, 2012

sitive (> 70 %), while the sensitivity over continental regions is on the order of 10–30 %, which is consistent with some previous estimates. While the simplifying assumptions employed by past CCN closure studies produce significant overprediction of N_{CCN} when compared to observations, the impact of these uncertainties on the prediction of N_d is on the order of ±10 % over most of the continental United States, but as high as 30–50 % in the Alaskan Arctic, Houston, TX, and Los Angeles, CA, where the highest N_{CCN} prediction uncertainties were observed.

This work shows that the regional sensitivity of N_d to N_{CCN} is important when assessing the uncertainty in cloud droplet number and albedo, and hence indirect forcing, associated with simplified assumptions regarding CCN. Most CCN closure studies to date have been located in continental regions, and future measurements of CCN and aerosol properties should focus on more remote regions to improve the coverage of the global dataset. Much of the past global anthropogenic indirect forcing has been over the continents, and the results of this study indicate that uncertainties in estimating the global aerosol indirect effect arising from the simplified composition assumptions in models are relatively small. Two questions remain, however, that motivate future research. First, climate models may employ prescribed size distributions for aerosol composition modes, which are likely to be a large source of uncertainty; however, the closure studies employed in this study use measured size distribution information. Consequently, size distribution effects are not reflected in the ΔN_{CCN} proxy. Second, the impact of transient events such as long-range pollution transport or seasonal biogenic emissions sources on changing CCN concentrations remains unclear; the regional sensitivities uncovered in this study indicate that these events could have a substantial climatic impact. This motivates future field measurements directed at measuring CCN in the southern oceans and Arctic, where observations are limited and seasonal variations have been shown to be significant. These datasets would provide important information to quantify the impact of, and uncertainty associated with, how transient pollution events might influence predictions of CCN concentrations, and hence, clouds and climate.

ACPD
12, 20483–20517, 2012

Acknowledgements. RHM acknowledges support from a NASA Postdoctoral Program fellowship and an ESS graduate research fellowship. SLC also acknowledges support from a NASA ESS graduate research fellowship.

References

Abdul-Razzak, H., Ghan, S. J., and Rivera-Carpio, C.: A parameterization of aerosol activation: 1. single aerosol type, J. Geophys. Res., 103, 6123–6131, doi:10.1029/97JD03735, 1998. 20487

Acker, J. G. and Leptoukh, G.: Online analysis enhances use of NASA Earth science data, EOS Trans. Am. Geophys. Union, 88, p. 14, doi:10.1029/2007EO020003, 2007. 20495

Anderson, B. E., Grant, W. B., Gregory, G. L., Browell, E. V., James E. Collins, J., Sachse, G. W., Bagwell, D. R., Hudgins, C. H., Blake, D. R., and Blake, N. J.: Aerosols from biomass burning over the Tropical South Atlantic region: distributions and impacts, J. Geophys. Res., 101, 24117–24137, doi:10.1029/96JD00717, 1996. 20491

Asa-Awuku, A., Moore, R. H., Nenes, A., Bahreini, R., Holloway, J. S., Brock, C. A., Middlebrook, A. M., Ryerson, T. B., Jimenez, J. L., DeCarlo, P. F., Hecobian, A., Weber, R. J., Stickel, R., Tanner, D. J., and Huey, L. G.: Airborne cloud condensation nuclei measurements during the 2006 Texas Air Quality Study, J. Geophys. Res., 116, D11201, doi:10.1029/2010JD014874, 2011. 20510

Barahona, D. and Nenes, A.: Parameterization of cloud droplet formation in large-scale models: including effects of entrainment, J. Geophys. Res., 112, D16206, doi:10.1029/2007JD008473, 2007. 20492

Bougiatioti, A., Fountoukis, C., Kalivitis, N., Pandis, S. N., Nenes, A., and Mihalopoulos, N.: Cloud condensation nuclei measurements in the marine boundary layer of the Eastern Mediterranean: CCN closure and droplet growth kinetics, Atmos. Chem. Phys., 9, 7053–7066, doi:10.5194/acp-9-7053-2009, 2009. 20510

Bougiatioti, A., Nenes, A., Fountoukis, C., Kalivitis, N., Pandis, S. N., and Mihalopoulos, N.: Size-resolved CCN distributions and activation kinetics of aged continental and marine aerosol, Atmos. Chem. Phys., 11, 8791–8808, doi:10.5194/acp-11-8791-2011, 2011. 20510

ACPD

12, 20483–20517, 2012

Broekhuizen, K., Chang, R.Y.-W., Leaitch, W. R., Li, S.-M., and Abbatt, J. P. D.: Closure between measured and modeled cloud condensation nuclei (CCN) using size-resolved aerosol compositions in downtown Toronto, Atmos. Chem. Phys., 6, 2513–2524, doi:10.5194/acp-6-2513-2006, 2006. 20510

Cai, Y., Montague, D. C., Mooiweer-Bryan, W., and Deshler, T.: Performance characteristics of the ultra high sensitivity aerosol spectrometer for particles between 55 and 800 nm: laboratory and field studies, J. Aerosol Sci., 39, 759–769, doi:10.1016/j.jaerosci.2008.04.007, 2008. 20485

Chang, R. Y.-W., Liu, P. S. K., Leaitch, W. R., and Abbatt, J. P. D.: Comparison between measured and predicted CCN concentrations at Egbert, Ontario: focus on the organic aerosol fraction at a semi-rural site, Atmos. Environ., 41, 8172–8182, doi:10.1016/j.atmosenv.2007.06.039, 2007. 20510

Chang, R. Y.-W., Slowik, J. G., Shantz, N. C., Vlasenko, A., Liggio, J., Sjostedt, S. J., Leaitch, W. R., and Abbatt, J. P. D.: The hygroscopicity parameter (κ) of ambient organic aerosol at a field site subject to biogenic and anthropogenic influences: relationship to degree of aerosol oxidation, Atmos. Chem. Phys., 10, 5047–5064, doi:10.5194/acp-10-5047-2010, 2010. 20510

Chuang, P. Y., Charlson, R. J., and Seinfeld, J. H.: Kinetic limitations on droplet formation in clouds, Nature, 390, 594–596, doi:10.1038/37576, 1997. 20491

Chuang, P. Y., Collins, D. R., Pawlowska, H., Snider, J. R., Jonsson, H. H., Brenguier, J. L., Flagan, R. C., and Seinfeld, J. H.: CCN measurements during ACE-2 and their relationship to cloud microphysical properties, Tellus, 52, 843–867, doi:10.1034/j.1600-0889.2000.00018.x, 2000. 20486, 20492

Conant, W. C., VanReken, T. M., Rissman, T. A., Varutbangkul, V., Jonsson, H. H., Nenes, A., Jimenez, J. L., Delia, A. E., Bahreini, R., Roberts, G. C., Flagan, R. C., and Seinfeld, J. H.: Aerosol–cloud drop concentration closure in warm cumulus, J. Geophys. Res., 109, D13204, doi:10.1029/2003JD004324, 2004. 20486

Considine, D. B., Bergmann, D. J., and Liu, H.: Sensitivity of Global Modeling Initiative chemistry and transport model simulations of radon-222 and lead-210 to input meteorological data, Atmos. Chem. Phys., 5, 3389–3406, doi:10.5194/acp-5-3389-2005, 2005. 20491

Covert, D. S., Gras, J. L., Wiedensohler, A., and Stratmann, F.: Comparison of directly measured CCN with CCN modeled from the number-size distribution in the marine bound-

ACPD
12, 20483–20517, 2012

ary layer during ACE 1 at Cape Grim, Tasmania, J. Geophys. Res., 103, 16597–16608, doi:10.1029/98JD01093, 1998. 20490

Cruz, C. N. and Pandis, S. N.: A study of the ability of pure secondary organic aerosol to act as cloud condensation nuclei, Atmos. Environ., 31, 2205–2214, doi:10.1016/S1352-2310(97)00054-X, 1997. 20485

Cubison, M. J., Ervens, B., Feingold, G., Docherty, K. S., Ulbrich, I. M., Shields, L., Prather, K., Hering, S., and Jimenez, J. L.: The influence of chemical composition and mixing state of Los Angeles urban aerosol on CCN number and cloud properties, Atmos. Chem. Phys., 8, 5649–5667, doi:10.5194/acp-8-5649-2008, 2008. 20497, 20510

d'Almeida, G. A.: On the variability of desert aerosol radiative characteristics, J. Geophys. Res., 92, 3017–3026, doi:10.1029/JD092iD03p03017, 1987. 20491

Dusek, U., Covert, D. S., Wiedensohler, A., Neusüss, C., Weise, D., and Cantrell, W.: Cloud condensation nuclei spectra derived from size distributions and hygroscopic properties of the aerosol in Coastal South-West Portugal during ACE-2, Tellus, 55, 35–53, doi:10.1034/j.1600-0889.2003.00041.x, 2003. 20490

Ervens, B., Cubison, M., Andrews, E., Feingold, G., Ogren, J. A., Jimenez, J. L., DeCarlo, P., and Nenes, A.: Prediction of cloud condensation nucleus number concentration using measurements of aerosol size distributions and composition and light scattering enhancement due to humidity, J. Geophys. Res., 112, D10S32, doi:10.1029/2006JD007426, 2007. 20510

Ervens, B., Cubison, M. J., Andrews, E., Feingold, G., Ogren, J. A., Jimenez, J. L., Quinn, P. K., Bates, T. S., Wang, J., Zhang, Q., Coe, H., Flynn, M., and Allan, J. D.: CCN predictions using simplified assumptions of organic aerosol composition and mixing state: a synthesis from six different locations, Atmos. Chem. Phys., 10, 4795–4807, doi:10.5194/acp-10-4795-2010, 2010. 20487, 20490, 20497, 20498, 20510

Flagan, R. C.: Opposed migration aerosol classifier (OMAC), Aerosol Sci. Tech., 38, 890–899, doi:10.1080/027868290505242, 2004. 20485

Fountoukis, C. and Nenes, A.: Continued development of a cloud droplet formation parameterization for global climate models, J. Geophys. Res., 110, D11212, doi:10.1029/2004JD005591, 2005. 20492

Fountoukis, C., Nenes, A., Meskhidze, N., Bahreini, R., Conant, W. C., Jonsson, H., Murphy, S., Sorooshian, A., Varutbangkul, V., Brechtel, F., Flagan, R. C., and Seinfeld, J. H.: Aerosol-cloud drop concentration closure for clouds sampled during the international consortium for

ACPD
12, 20483–20517, 2012

atmospheric research on transport and transformation 2004 campaign, J. Geophys. Res., 112, D10S30, doi:10.1029/2006JD007272, 2007. 20486, 20492
Gasparini, R., Collins, D. R., Andrews, E., Sheridan, P. J., Ogren, J. A., and Hudson, J. G.: Coupling aerosol size distributions and size-resolved hygroscopicity to predict humidity-dependent optical properties and cloud condensation nuclei spectra, J. Geophys. Res., 111, D05S13, doi:10.1029/2005JD006092, 2006. 20490
Giebl, H., Berner, A., Reischl, G., Puxbaum, H., Kasper-Giebl, A., and Hitzenberger, R.: CCN activation of oxalic and malonic acid test aerosols with the University of Vienna cloud condensation nuclei, J. Aerosol Sci., 33, 1623–1634, doi:10.1016/S0021-8502(02)00115-5, 2002. 20485
Good, N., Topping, D. O., Allan, J. D., Flynn, M., Fuentes, E., Irwin, M., Williams, P. I., Coe, H., and McFiggans, G.: Consistency between parameterisations of aerosol hygroscopicity and CCN activity during the RHaMBLe discovery cruise, Atmos. Chem. Phys., 10, 3189–3203, doi:10.5194/acp-10-3189-2010, 2010. 20490
Guibert, S., Snider, J. R., and Brenguier, J.-L.: Aerosol activation in marine stratocumulus clouds: 1. measurement validation for a closure study, J. Geophys. Res., 108, 8628, doi:10.1029/2002JD002678, 2003. 20492
Gunthe, S. S., King, S. M., Rose, D., Chen, Q., Roldin, P., Farmer, D. K., Jimenez, J. L., Artaxo, P., Andreae, M. O., Martin, S. T., and Pöschl, U.: Cloud condensation nuclei in pristine tropical rainforest air of Amazonia: size-resolved measurements and modeling of atmospheric aerosol composition and CCN activity, Atmos. Chem. Phys., 9, 7551–7575, doi:10.5194/acp-9-7551-2009, 2009. 20510
Hallberg, A., Wobrock, W., Flossmann, A. I., Bower, K. N., Noone, K. J., Wiedensohler, A., Hansson, H.-C., Wendisch, M., Berner, A., Kruisz, C., Laj, P., Facchini, M. C., Fuzzi, S., and Arends, B. G.: Microphysics of clouds: model versus measurements, Atmos. Environ., 31, 2453–2462, doi:10.1016/S1352-2310(97)00041-1, 1997. 20486
Hudson, J. G.: Cloud condensation nuclei, J. Appl. Meteorol., 32, 596–607, doi:10.1175/1520-0450(1993)032<0596:CCN>2.0.CO;2, 1993. 20485
Jayne, J. T., Leard, D. C., Zhang, X., Davidovits, P., Smith, K. A., Kolb, C. A., and Worsnop, D. R.: Development of an aerosol mass spectrometer for size and composition analysis of submicron particles, Aerosol Sci. Tech., 33, 49–70, doi:10.1080/027868200410840, 2000. 20485
Jimenez, J. L., Jayne, J. T., Shi, Q., Kolb, C. E., Worsnop, D. R., Yourshaw, I., Seinfeld, J. H., Flagan, R. C., Zhang, X., Smith, K. A., Morris, J. W., and Davidovits, P.: Ambient aerosol

ACPD
12, 20483–20517, 2012

sampling using the Aerodyne Aerosol Mass Spectrometer, J. Geophys. Res., 108, 8425, doi:10.1029/2001JD001213, 2003. 20485

Jurányi, Z., Gysel, M., Weingartner, E., DeCarlo, P. F., Kammermann, L., and Baltensperger, U.: Measured and modelled cloud condensation nuclei number concentration at the high alpine site Jungfraujoch, Atmos. Chem. Phys., 10, 7891–7906, doi:10.5194/acp-10-7891-2010, 2010. 20510

Kammermann, L., Gysel, M., Weingartner, E., Herich, H., Cziczo, D. J., Holst, T., Svenningsson, B., Ameth, A., and Baltensperger, U.: Subarctic atmospheric aerosol composition: 3. measured and modeled properties of cloud condensation nuclei, J. Geophys. Res., 115, D04202, doi:10.1029/2009JD012447, 2010. 20490

Karydis, V. A., Kumar, P., Barahona, D., Sokolik, I. N., and Nenes, A.: On the effect of dust particles on global CCN and cloud droplet number, J. Geophys. Res., 116, D23204, doi:10.1029/2011JD016283, 2011. 20492, 20493

Karydis, V. A., Capps, S. L., Russell, A. G., and Nenes, A.: Adjoint sensitivity of global cloud droplet number to aerosol and dynamical parameters, Atmos. Chem. Phys. Discuss., 12, 12081–12117, doi:10.5194/acpd-12-12081-2012, 2012. 20488, 20491, 20492, 20494

Kim, J. H., Yum, S. S., Shim, S., Yoon, S.-C., Hudson, J. G., Park, J., and Lee, S.-J.: On aerosol hygroscopicity, cloud condensation nuclei (CCN) spectra and critical supersaturation measured at two remote islands of Korea between 2006 and 2009, Atmos. Chem. Phys., 11, 12627–12645, doi:10.5194/acp-11-12627-2011, 2011. 20490

Koch, D. and Rind, D.: Beryllium 10/beryllium 7 as a tracer of stratospheric transport, J. Geophys. Res., 103, 3907–3917, doi:10.1029/97JD03117, 1998. 20492

Köhler, H.: The nucleus in and growth of hygroscopic droplets, T. Faraday Soc., 32, 1152–1161, doi:10.1039/TF9363201152, 1936. 20485

Koren, I. and Feingold, G.: Aerosol-cloud-precipitation system as a predator-prey problem, P. Natl. Acad. Sci. USA, 108, 12227–12232, doi:10.1073/pnas.1101777108, 2011. 20496

Kumar, P., Sokolik, I. N., and Nenes, A.: Parameterization of cloud droplet formation for global and regional models: including adsorption activation from insoluble CCN, Atmos. Chem. Phys., 9, 2517–2532, doi:10.5194/acp-9-2517-2009, 2009. 20488, 20491, 20492

Kuwata, M., Kondo, Y., Miyazaki, Y., Komazaki, Y., Kim, J. H., Yum, S. S., Tanimoto, H., and Matsueda, H.: Cloud condensation nuclei activity at Jeju Island, Korea in spring 2005, Atmos. Chem. Phys., 8, 2933–2948, doi:10.5194/acp-8-2933-2008, 2008. 20510

ACPD

12, 20483–20517, 2012

Lance, S., Nenes, A., and Rissman, T. A.: Chemical and dynamical effects on cloud droplet number: implications for estimates of the aerosol indirect effect, J. Geophys. Res., 109, D22208, doi:10.1029/2004JD004596, 2004. 20486, 20491

Lance, S., Medina, J., Smith, J. N., and Nenes, A.: Mapping the operation of the DMT continuous-flow CCN counter, Aerosol Sci. Tech., 40, 242–254, doi:10.1080/02786820500543290, 2006. 20485

Lance, S., Nenes, A., Mazzoleni, C., Dubey, M. K., Gates, H., Varutbangkul, V., Rissman, T. A., Murphy, S. M., Sorooshian, A., Flagan, R. C., Seinfeld, J. H., Feingold, G., and Jonsson, H. H.: Cloud condensation nuclei activity, closure, and droplet growth kinetics of Houston aerosol during the Gulf of Mexico Atmospheric Composition and Climate Study (GoMACCS), J. Geophys. Res., 114, D00F15, doi:10.1029/2008JD011699, 2009. 20510

Lathem, T. L., Beyersdorf, A. J., Thornhill, L., Winstead, E., Cubison, M. J., Hecobian, A., Jimenez, J. L., Weber, R. J., Anderson, B. E., and Nenes, A.: Analysis of the CCN activity of Canadian biomass burning and Arctic aerosol during Summer 2008, Atmos. Chem. Phys. Discuss, in preparation, 2012. 20510

Lee, L. A., Carslaw, K. S., Pringle, K. J., Mann, G. W., and Spracklen, D. V.: Emulation of a complex global aerosol model to quantify sensitivity to uncertain parameters, Atmos. Chem. Phys., 11, 12253–12273, doi:10.5194/acp-11-12253-2011, 2011. 20488

Liu, X., Penner, J. E., and Herzog, M.: Global modeling of aerosol dynamics model description, evaluation, and interactions between sulfate and nonsulfate aerosols, J. Geophys. Res., 110, D18206, doi:10.1029/2004JD005674, 2005. 20491

Martin, M., Chang, R. Y.-W., Sierau, B., Sjogren, S., Swietlicki, E., Abbatt, J. P. D., Leck, C., and Lohmann, U.: Cloud condensation nuclei closure study on summer arctic aerosol, Atmos. Chem. Phys., 11, 11335–11350, doi:10.5194/acp-11-11335-2011, 2011. 20510

Medina, J., Nenes, A., Sotirpoulou, R.-E. P., Cottrell, L. D., Ziemba, L. D., Beckman, P. J., and Griffin, R. J.: Cloud condensation nuclei closure during the international consortium for atmospheric research on transport and transformation 2004 campaign: effects of size-resolved composition, J. Geophys. Res., 112, D10S31, doi:10.1029/2006JD007588, 2007. 20487, 20510

Meskhidze, N., Nenes, A., Conant, W. C., and Seinfeld, J. H.: Evaluation of a new cloud droplet activation parameterization with in situ data from CRYSTAL-FACE and CSTRIPE, J. Geophys. Res., 110, D16202, doi:10.1029/2004JD005703, 2005. 20486, 20493

ACPD

12, 20483–20517, 2012

Moore, R. H., Bahreini, R., Brock, C. A., Froyd, K. D., Cozic, J., Holloway, J. S., Middlebrook, A. M., Murphy, D. M., and Nenes, A.: Hygroscopicity and composition of Alaskan Arctic CCN during April 2008, Atmos. Chem. Phys., 11, 11807–11825, doi:10.5194/acp-11-11807-2011, 2011. 20497, 20510

Moore, R. H., Cerully, K., Bahreini, R., Brock, C. A., Middlebrook, A. M., and Nenes, A.: Hygroscopicity and composition of California CCN during Summer, 2010, J. Geophys. Res., 117, D00V12, doi:10.1029/2011JD017352, 2012a. 20497, 20510

Moore, R. H., Raatikainen, T., Langridge, J. M., Bahreini, R., Brock, C. A., Holloway, J. S., Lack, D. A., Middlebrook, A. M., Perring, A. E., Schwarz, J. P., Spackman, J. R., and Nenes, A.: CCN spectra, hygroscopicity, and droplet activation kinetics of secondary organic aerosol resulting from the 2010 Deepwater Horizon Oil Spill, Environ. Sci. Technol., 46, 3093–3100, doi:10.1021/es203362w, 2012b. 20510

Murphy, S. M., Agrawal, H., Sorooshian, A., Padró, L. T., Gates, H., Hersey, S., Welch, W. A., Jung, H., Miller, J. W., III, D. R. C., Nenes, A., Jonsson, H. H., Flagan, R. C., and Seinfeld, J. H.: Comprehensive simultaneous shipboard and airborne characterization of exhaust from a modern container ship at sea, Environ. Sci. Technol., 43, 4626–4640, doi:10.1021/es802413j, 2009. 20510

Nenes, A. and Seinfeld, J. H.: Parameterization of cloud droplet formation in global climate models, J. Geophys. Res., 108, 4415, doi:10.1029/2002JD002911, 2003. 20492

Olfert, J. S., Kulkarni, P., and Wang, J.: Measuring aerosol size distributions with the fast integrated mobility spectrometer, J. Aerosol Sci., 39, 940–956, doi:10.1016/j.jaerosci.2008.06.005, 2008. 20485

Paatero, J., Vaattovaara, P., Vestenius, M., Meinander, O., Makkonen, U., Kivi, R., Hyvärinen, A., Asmi, E., Tjernström, M., and Leck, C.: Finnish contribution to the Arctic Summer Cloud Ocean Study (ASCOS) expedition, Arctic Ocean 2008, Geophysica, 45, 119–146, 2009. 20510

Padró, L. T., Asa-Awuku, A., Morrison, R., and Nenes, A.: Inferring thermodynamic properties from CCN activation experiments: single-component and binary aerosols, Atmos. Chem. Phys., 7, 5263–5274, doi:10.5194/acp-7-5263-2007, 2007. 20485

Padró, L. T., Moore, R. H., Zhang, X., Rastogi, N., Weber, R. J., and Nenes, A.: Mixing state and compositional effects on CCN activity and droplet growth kinetics of size-resolved CCN in an urban environment, Atmos. Chem. Phys. Discuss., in review, 2012. 20510

ACPD
12, 20483–20517, 2012

Petters, M. D. and Kreidenweis, S. M.: A single parameter representation of hygroscopic growth and cloud condensation nucleus activity, Atmos. Chem. Phys., 7, 1961–1971, doi:10.5194/acp-7-1961-2007, 2007. 20489

Quinn, P. K., Bates, T. S., Coffman, D. J., and Covert, D. S.: Influence of particle size and chemistry on the cloud nucleating properties of aerosols, Atmos. Chem. Phys., 8, 1029–1042, doi:10.5194/acp-8-1029-2008, 2008. 20510

Radke, L. F., Hegg, D. A., Lyons, J. H., Brock, C. A., Hobbs, P. V., Weiss, R., and Rasmussen, R.: Aerosols and Climate, chap. Airborne measurements on smokes from biomass burning, Deepak Publishing, Hampton, VA, USA, 411–422, 1988. 20491

Raymond, T. M. and Pandis, S. N.: Cloud activation of single-component organic aerosol particles, J. Geophys. Res., 107, 4787, doi:10.1029/2002JD002159, 2002. 20485

Raymond, T. M. and Pandis, S. N.: Formation of cloud droplets by multicomponent organic particles, J. Geophys. Res., 108, 4469, doi:10.1029/2003JD003503, 2003. 20485

Rind, D. and Lerner, J.: Use of on-line tracers as a diagnostic tool in general circulation model development, 1. Horizontal and vertical transport in the troposphere, J. Geophys. Res., 101, 12667–12683, doi:10.1029/96JD00551, 1996. 20492

Rissman, T. A., Nenes, A., and Seinfeld, J. H.: Chemical amplification (or dampening) of the Twomey effect: conditions derived from droplet activation theory, J. Atmos. Sci., 61, 919–930, doi:10.1175/1520-0469(2004)061<0919:CAODOT>2.0.CO;2, 2004. 20487

Rissman, T. A., VanReken, T. M., Wang, J., Gasparini, R., Collins, D. R., Jonsson, H. H., Brechtel, F. J., Flagan, R. C., and Seinfeld, J. H.: Characterization of ambient aerosol from measurements of cloud condensation nuclei during 2003 atmospheric radiation measurement aerosol intensive observational period at the Southern Great Plains site in Oklahoma, J. Geophys. Res., 111, D05S11, doi:10.1029/2004JD005695, 2006. 20510

Roberts, G., Mauger, G., Hadley, O., and Ramanathan, V.: North American and Asian aerosols over the Eastern Pacific Ocean and their role in regulating cloud condensation nuclei, J. Geophys. Res., 111, D13205, doi:10.1029/2005JD006661, 2006. 20510

Roberts, G. C. and Nenes, A.: A continuous-flow streamwise thermal-gradient CCN chamber for atmospheric measurements, Aerosol Sci. Tech., 39, 206–221, doi:10.1080/027868290913988, 2005. 20485

Rose, D., Gunthe, S. S., Su, H., Garland, R. M., Yang, H., Berghof, M., Cheng, Y. F., Wehner, B., Achtert, P., Nowak, A., Wiedensohler, A., Takegawa, N., Kondo, Y., Hu, M., Zhang, Y., Andreae, M. O., and Pöschl, U.: Cloud condensation nuclei in polluted air and biomass burn-

ACPD
12, 20483–20517, 2012

ing smoke near the mega-city Guangzhou, China – Part 2: Size-resolved aerosol chemical composition, diurnal cycles, and externally mixed weakly CCN-active soot particles, Atmos. Chem. Phys., 11, 2817–2836, doi:10.5194/acp-11-2817-2011, 2011. 20510

Rotman, D. A., Tannahill, J. R., Kinnison, D. E., Connell, P. S., Bergmann, D., Proctor, D., Rodriguez, J. M., Lin, S. J., Rood, R. B., Prather, M. J., Rasch, P. J., Considine, D. B., Ramaroson, R., and Kawa, S. R.: Global modeling initiative assessment model: model description, integration, and testing of the transport shell, J. Geophys. Res., 106, 1669–1691, doi:10.1029/2000JD900463, 2001. 20491

Snider, J. R. and Brenguier, J.-L.: Cloud condensation nuclei and cloud droplet measurements during ACE-2, Tellus, 52, 828–842, doi:10.1034/j.1600-0889.2000.00044.x, 2000. 20486

Snider, J. R., Guibert, S., Brenguier, J.-L., and Putaud, J.-P.: Aerosol activation in marine stratocumulus clouds: 2. Köhler and parcel theory closure studies, J. Geophys. Res., 108, 8629, doi:10.1029/2002JD002692, 2003. 20486

Solomon, S., Qin, D., Manning, M., Chen, Z., Marquis, M., Averyt, K. B., Tignor, M., and Miller, H. L. (eds.): Climate Change 2007: The Physical Science Basis, Intergovernmental Panel on Climate Change Fourth Assessment Report, Cambridge University Press, New York, NY, USA, 2007. 20485

Sotiropoulou, R.-E. P., Medina, J., and Nenes, A.: CCN predictions: is theory sufficient for assessments of the indirect effect?, Geophys. Res. Lett., 33, L05816, doi:10.1029/2005GL025148, 2006. 20487

Sotiropoulou, R.-E. P., Nenes, A., Adams, P. J., and Seinfeld, J. H.: Cloud condensation nuclei prediction error from application of Köhler theory: importance for the aerosol indirect effect, J. Geophys. Res., 112, D12202, doi:10.1029/2006JD007834, 2007. 20487, 20495, 20498

Stevens, B. and Feingold, G.: Untangling aerosol effects on clouds and precipitation in a buffered system, Nature, 461, 607–613, doi:10.1038/nature08281, 2009. 20496

Stroud, C. A., Nenes, A., Jimenez, J. L., DeCarlo, P. F., Huffman, J. A., Bruintjes, R., Nemitz, E., Delia, A. E., Toohey, D. W., Guenther, A. B., and Nandi, S.: Cloud activating properties of aerosol observed during CELTIC, J. Atmos. Sci., 64, 441–459, doi:10.1175/JAS3843.1, 2007. 20510

Twomey, S.: The influence of pollution on the shortwave albedo of clouds, J. Atmos. Sci., 34, 1149–1152, doi:10.1175/1520-0469(1977)034<1149:TIOPOT>2.0.CO;2, 1977. 20485

Twomey, S.: Aerosols, clouds and radiation, Atmos. Environ., 25, 2435–2442, doi:10.1016/0960-1686(91)90159-5, 1991. 20496

ACPD
12, 20483–20517, 2012

VanReken, T. M., Rissman, T. A., Roberts, G. C., Varutbangkul, V., Jonsson, H. H., Flagan, R. C., and Seinfeld, J. H.: Toward aerosol/cloud condensation nuclei (CCN) closure during CRYSTAL-FACE, J. Geophys. Res., 108, 4633, doi:10.1029/2003JD003582, 2003. 20510

Vestin, A., Rissler, J., Swietlicki, E., Frank, G. P., and Andreae, M. O.: Cloud-nucleating properties of the Amazonian biomass burning aerosol: cloud condensation nuclei measurements and modeling, J. Geophys. Res., 112, D14201, doi:10.1029/2006JD008104, 2007. 20490

Wang, J., Lee, Y.-N., Daum, P. H., Jayne, J., and Alexander, M. L.: Effects of aerosol organics on cloud condensation nucleus (CCN) concentration and first indirect aerosol effect, Atmos. Chem. Phys., 8, 6325–6339, doi:10.5194/acp-8-6325-2008, 2008. 20510

Wang, J., Cubison, M. J., Aiken, A. C., Jimenez, J. L., and Collins, D. R.: The importance of aerosol mixing state and size-resolved composition on CCN concentration and the variation of the importance with atmospheric aging of aerosols, Atmos. Chem. Phys., 10, 7267–7283, doi:10.5194/acp-10-7267-2010, 2010. 20510

Wang, S. C. and Flagan, R. C.: Scanning electrical mobility spectrometer, J. Aerosol Sci., 20, 1485–1488, doi:10.1016/0021-8502(89)90868-9, 1989. 20485

Weber, R. J., Orsini, D., Daun, Y., Lee, Y.-N., Klotz, P. J., and Brechtel, F.: A particle-into-liquid collector for rapid measurement of aerosol bulk chemical composition, Aerosol Sci. Tech., 35, 718–727, doi:10.1080/02786820152546761, 2001. 20485

Yum, S. S., Roberts, G., Kim, J. H., Song, K., and Kim, D.: Submicron aerosol size distributions and cloud condensation nuclei concentrations measured at Gosan, Korea, during the Atmospheric Brown Clouds–East Asian Regional Experiment 2005, J. Geophys. Res., 112, D22S32, doi:10.1029/2006JD008212, 2007. 20510

ACPD

12, 20483–20517, 2012

Table 1. Summary of past CCN closure studies using measured aerosol compositions and size distributions for predictions.

	Study Location	Dates	GPS Coordinates Latitude	Longitude	Observed N_{CCN} (cm^{-3})	Observed s (%)	Reference
1	Arctic (Alaskan), Spring Background (ARCPAC)	04/2008	65–76° N	130–163° W	100–500	0.1–0.3	Moore et al. (2011)
2	Arctic (N. Atlantic), Summer (ASCOS)	08/2008–09/2008	78–88° N	12° W–16° E	0–200	0.10–0.73	Martin et al. (2011); Paatero et al. (2009)
3	Amazon Rainforest, Brazil (AMAZE-08)	02/2008–03/2008	−3–10° N	50–60° W	40–200	0.10–0.82	Gunthe et al. (2009)
4	Atlanta, GA (AMIGAS)	07/2008–08/2008	33–34° N	84–85° W	500–10 000	0.2–1.0	Padró et al. (2012)
5	Chebogue Point, Canada (ICARTT)	07/2004–08/2004	43–44° N	62–63° W	0–4000	0.65	Ervens et al. (2007, 2010)
6	Canadian Arctic, Summer Background (ARCTAS)	06/2008–07/2008	66–85° N	40–130° W	100–500	0.2–0.57	Lathem et al. (2012)
7	Canadian Arctic, Fresh Biomass Burning (ARCTAS)	06/2008–07/2008	50–57° N	85–120° W	2000–25 000	0.2–0.57	Lathem et al. (2012)
8	Duke Forest, NC (Celtic)	07/2003	34–36° N	75–80° W	0–3000	0.20–0.33	Stroud et al. (2007)
9	Ebert, Ontario, Canada (CARE)	11/2005	43–45° N	79–81° W	400–5000	0.32	Chang et al. (2007)
10	Ebert, Ontario, Canada (CARE)	05/2007–06/2007	43–45° N	79–81° W	0–10 000	0.42	Chang et al. (2010)
11	Finokalia, Greece (FAME-07)	06/2007–10/2007	33–38° N	15–25° E	500–4000	0.21–0.73	Bougiatioti et al. (2009, 2011)
12	Florida Coast (CRYSTAL-FACE)	07/2002	24–27° N	80–84° W	230–380	0.20–0.85	VanReken et al. (2003)
13	Guangzhou, China (PRIDE-PRD2006)	07/2006	21–24° N	111–115° E	1000–10 000	0.068–0.47	Rose et al. (2011)
14	Gulf Coast, Houston, TX (GoMAACS)	08/2006–09/2006	27–29° N	93–95° W	3000–30 000	0.44	Quinn et al. (2008); Ervens et al. (2010)
15	Gulf of Mexico Background Air (CalNex)	06/2010	27–31° N	84–86° W	100–2500	0.33	Moore et al. (2012b), Unpublished Data
16	Holme Moss, UK	11/2006–12/2006	53–54° N	4–5° W	400–1200	0.23	Ervens et al. (2010)
17	Houston, TX (GoMACCS)	08/2006–09/2006	29–32° N	93–97° W	200–15 000	0.35–1.0	Lance et al. (2009)
18	Houston, TX (TexAQS)	09/2006–10/2006	29–34° N	92–100° W	200–2000	0.30–0.71	Asa-Awuku et al. (2011)
19	Jeju Island, Korea (ABC-EAREX)	03/2005–04/2005	32–36° N	124–128° E	1500–3500	0.6	Yum et al. (2007)
20	Jeju Island, Korea (ABC-EAREX)	03/2005–04/2005	32–36° N	124–128° E	400–4600	0.09–0.97	Kuwata et al. (2008)
21	Jungfraujoch, Switzerland	05/2008	46–47° N	7–9° E	0–1500	0.12–1.18	Jurányi et al. (2010)
22	Los Angeles, CA (CalNex)	05/2010–06/2010	33–35° N	116–118° W	0–7000	0.25–0.65	Moore et al. (2012a)
23	Mexico City, Mexico (MILAGRO)	03/2006	19–20° N	98–100° W	7000–17 000	0.29	Wang et al. (2010); Ervens et al. (2010)
24	Monterey, CA (MASE)	07/2005	36–39° N	121–125° W	300–1300	0.1	Ervens et al. (2010)
25	Monterey, CA, Above Cloud (MASE)	07/2005	36–39° N	121–125° W	0–1700	0.2	Wang et al. (2008)
26	Monterey, CA, Marine Boundary Layer (MASE)	07/2005	36–39° N	121–125° W	0–1700	0.2	Wang et al. (2008)
27	Pacific (Eastern), N. California Coast (CIFEX)	04/2004	37–44° N	123–130° W	200–1000	0.2–0.8	Roberts et al. (2006)
28	Pacific (Eastern), Los Angeles, CA (CalNex)	05/2010–06/2010	33–34° N	118–120° W	50–6000	0.25–0.65	Moore et al. (2012a)
29	Riverside, CA (SOAR-I)	07/2005–08/2005	33–34° N	116–119° W	11 000–19 000	0.27	Cubison et al. (2008); Ervens et al. (2010)
30	San Joaquin Valley, CA (CalNex)	05/2010–06/2010	35–38° N	118–121° W	100–8000	0.25–0.65	Moore et al. (2012a)
31	Sacramento Valley, CA (CalNex)	05/2010–06/2010	38–40° N	121–123° W	50–7000	0.25–0.65	Moore et al. (2012a)
32	Ship Channel, Houston, TX (GoMACCS)	08/2006–09/2006	28–30° N	94–95° W	400–3000	0.44	Quinn et al. (2008); Ervens et al. (2010)
33	Ship Exhaust Plume, Monterey, CA (MASE-II)	07/2007	35–36° N	123–124° W	200–30 000	0.10–0.35	Murphy et al. (2009)
34	Southern Great Plains ARM Site, OK	05/2003	35–37° N	96–98° W	100–11 000	2.1–2.8	Rissman et al. (2006)
35	Thompson Farms, NH (ICARTT)	08/2004	42–44° N	70–74° W	100–4000	0.2–0.6	Medina et al. (2007)
36	Toronto, Canada	09/2003	43–44° N	79–80° W	0–3500	0.58	Broekhuizen et al. (2006)

ACPD
12, 20483–20517, 2012

Table 2. CCN number concentration percent overprediction $(\Delta N_{CCN}/N_{CCN}) \times 100\,\%$ for different closure scenarios reported by the studies in Table 1.

	Study Location	Internal Mixture				External Mixture	
		$(NH_4)_2SO_4$	Sol. Org.	Insol. Org.	Size-Dep.	Sol. Org.	Insol. Org.
1	Arctic (Alaskan), Spring Background (ARCPAC)	69 ± 65	57 ± 50	49 ± 47	–	11 ± 30	−23 ± 36
2	Arctic (N. Atlantic), Summer (ASCOS)	–	−6–43 ± 21	–	–	–	–
3	Amazon Rainforest, Brazil (AMAZE-08)	–	14.1	–	–	–	–
4	Atlanta, GA (AMIGAS)	194	157	146	–	169	40
5	Chebogue Point, Canada (ICARTT)	–	40 ± 40	−10 ± 40	–	20 ± 30	−30 ± 30
6	Canadian Arctic, Summer Background (ARCTAS)	–	12 ± 21	−27 ± 16	–	−1 ± 20	–
7	Canadian Arctic, Fresh Biomass Burning (ARCTAS)	–	2 ± 24	−44 ± 16	–	−9 ± 23	–
8	Duke Forest, NC (Celtic)	–	71	20	–	–	–
9	Ebert, Ontario, Canada (CARE)	–	−29	–	−14	–	–
10	Ebert, Ontario, Canada (CARE)	–	–	−3	–	–	–
11	Finokalia, Greece (FAME-07)	–	1.8 ± 12	−2.8 ± 14	−7 ± 11	–	–
12	Florida Coast (CRYSTAL-FACE)	6	–	–	–	–	–
13	Guangzhou, China (PRIDE-PRD2006)	–	20.7	–	–	–	–
14	Gulf Coast, Houston, TX (GoMAACS)	–	130 ± 190	70 ± 100	–	140 ± 190	90 ± 110
15	Gulf of Mexico Background Air (CalNex)	41 ± 26	19 ± 16	13 ± 14	–	5 ± 18	−39 ± 20
16	Holme Moss, UK	–	−10 ± 50	−20 ± 50	–	20 ± 60	0 ± 50
17	Houston, TX (GoMACCS)	36.5	–	2.6	–	–	–
18	Houston, TX (TexAQS)	11.6 ± 9.3	−3.6 ± 7.7	−16.1 ± 10.0	−13.1 ± 8.4	–	−60.9 ± 6.4
19	Jeju Island, Korea (ABC-EAREX)	27 ± 29	–	–	–	–	–
20	Jeju Island, Korea (ABC-EAREX)	16 ± 18	–	–	–	–	–
21	Jungfraujoch, Switzerland	–	4 ± 3	–	–	–	–
22	Los Angeles, CA (CalNex)	84 ± 97	54 ± 57	41 ± 51	18 ± 85	38 ± 49	−16 ± 42
23	Mexico City, Mexico (MILAGRO)	–	10 ± 20	−50 ± 20	10	10 ± 10	−50 ± 20
24	Monterey, CA (MASE)	–	10 ± 60	10 ± 60	–	30 ± 60	30 ± 60
25	Monterey, CA, Above Cloud (MASE)	−54	17	−29	–	−11	−78
26	Monterey, CA, Marine Boundary Layer (MASE)	−8	–	−5	–	–	–
27	Pacific (Eastern), N. California Coast (CIFEX)	79	–	–	–	–	–
28	Pacific (Eastern), Los Angeles, CA (CalNex)	58 ± 90	32 ± 39	23 ± 34	−5 ± 31	20 ± 36	−23 ± 33
29	Riverside, CA (SOAR-I)	–	500 ± 210	360 ± 170	–	390 ± 170	340 ± 180
30	San Joaquin Valley, CA (CalNex)	141 ± 187	71 ± 154	45 ± 126	28 ± 75	56 ± 132	2 ± 67
31	Sacramento Valley, CA (CalNex)	150 ± 190	25 ± 29	−3 ± 26	−14 ± 77	16 ± 25	−59 ± 22
32	Ship Channel, Houston, TX (GoMACCS)	–	320 ± 320	300 ± 300	–	300 ± 300	140 ± 190
33	Ship Exhaust Plume, Monterey, CA (MASE-II)	–	–	23 ± 6	16 ± 6	–	–
34	Southern Great Plains ARM Site, OK	92 ± 192	–	–	–	–	–
35	Thompson Farms, NH (ICARTT)	–	–	35.7 ± 28.5	17.4 ± 27.1	–	–
36	Toronto, Canada	–	–	–	12	–	–
Number of studies		16	25	25	11	17	16

ACPD
12, 20483–20517, 2012

Table 3. Comparison of regional observed CCN number concentration, N_{CCN}; simulated aerosol number concentration, N_a; simulated cloud droplet concentration, N_d; the normalized cloud droplet concentration sensitivity, $\left(\frac{\partial N_d}{\partial N_a}\right)\left(\frac{N_a}{N_d}\right)$; and semi-normalized Albedo sensitivity $\left(\frac{\partial N_d}{\partial N_a}\right)N_a$. All reported results are annual arithmetic means (± one standard deviation), except for N_a and N_d, which are geometric means ($\overset{\times}{\div}$ one geometric standard deviation).

	Study Location	Observed s (%)	Observed N_{CCN} (cm^{-3})	Simulated N_a (cm^{-3})	Simulated N_d (cm^{-3})	$\left(\frac{\partial N_d}{\partial N_a}\right)\left(\frac{N_a}{N_d}\right)$	Satellite A	$\left(\frac{\partial A}{\partial N_a}\right)N_a$
1	Arctic (Alaskan), Spring Background (ARCPAC)	0.1–0.3	100–500	289	147	0.686	0.135	0.027
2	Arctic (N. Atlantic), Summer (ASCOS)	0.10–0.73	0–200	–	–	–	–	–
3	Amazon Rainforest, Brazil (AMAZE-08)	0.10–0.82	40–200	1022	226	0.459	0.111	0.014
4	Atlanta, GA (AMIGAS)	0.2–1.0	500–10 000	8292	612	0.121	0.136	0.005
5	Chebogue Point, Canada (ICARTT)	0.65	0–4000	2475	430	0.293	0.190	0.015
6	Canadian Arctic, Summer Background (ARCTAS)	0.2–0.57	100–500	378	196	0.669	0.096	0.019
7	Canadian Arctic, Fresh Biomass Burning (ARCTAS)	0.2–0.57	2000–25 000	1086	397	0.423	0.127	0.015
8	Duke Forest, NC (Celtic)	0.20–0.33	0–3000	7443	567	0.156	0.164	0.007
9	Ebert, Ontario, Canada (CARE)	0.32	400–5000	3103	520	0.205	0.175	0.010
10	Ebert, Ontario, Canada (CARE)	0.42	0–10 000	3103	520	0.205	0.175	0.010
11	Finokalia, Greece (FAME-07)	0.21–0.73	500–4000	8167	392	0.207	0.109	0.007
12	Florida Coast (CRYSTAL-FACE)	0.20–0.85	230–380	3377	348	0.295	0.119	0.010
13	Guangzhou, China (PRIDE-PRD2006)	0.068–0.47	1000–10 000	10 503	555	0.158	0.167	0.007
14	Gulf Coast, Houston, TX (GoMAACS)	0.44	3000–30 000	5960	434	0.269	0.142	0.011
15	Gulf of Mexico Background Air (CalNex)	0.33	100–2500	6741	548	0.172	0.135	0.007
16	Holme Moss, UK	0.23	400–1200	6364	378	0.309	0.191	0.016
17	Houston, TX (GoMACCS)	0.35–1.0	200–15 000	6668	496	0.212	0.142	0.009
18	Houston, TX (TexAQS)	0.30–0.71	200–2000	5919	522	0.192	0.133	0.007
19	Jeju Island, Korea (ABC-EAREX)	0.6	1500–3500	10 649	472	0.154	0.200	0.008
20	Jeju Island, Korea (ABC-EAREX)	0.09–0.97	400–4600	10 649	472	0.154	0.200	0.008
21	Jungfraujoch, Switzerland	0.12–1.18	0–1500	11 408	611	0.116	0.143	0.005
22	Los Angeles, CA (CalNex)	0.25–0.65	0–7000	1786	346	0.377	0.079	0.009
23	Mexico City, Mexico (MILAGRO)	0.29	7000–17 000	4178	518	0.197	0.118	0.007
24	Monterey, CA (MASE)	0.1	300–1300	1435	286	0.416	0.105	0.013
25	Monterey, CA, Above Cloud (MASE)	0.2	0–1700	1435	286	0.416	0.105	0.013
26	Monterey, CA, Marine Boundary Layer (MASE)	0.2	0–1700	1435	286	0.416	0.105	0.013
27	Pacific (Eastern), N. California Coast (CIFEX)	0.2–0.8	200–1000	866	126	0.447	0.155	0.019
28	Pacific (Eastern), Los Angeles, CA (CalNex)	0.25–0.65	50–6000	1558	229	0.418	0.098	0.013
29	Riverside, CA (SOAR-I)	0.27	11 000–19 000	1670	288	0.440	0.085	0.011
30	San Joaquin Valley, CA (CalNex)	0.25–0.65	100–8000	1710	409	0.326	0.088	0.009
31	Sacramento Valley, CA (CalNex)	0.25–0.65	50–7000	1435	286	0.416	0.105	0.013
32	Ship Channel, Houston, TX (GoMACCS)	0.44	400–3000	5960	434	0.269	0.142	0.011
33	Ship Exhaust Plume, Monterey, CA (MASE-II)	0.10–0.35	200–30 000	1441	213	0.491	0.111	0.016
34	Southern Great Plains ARM Site, OK	2.1–2.8	100–11 000	6313	603	0.128	0.128	0.005
35	Thompson Farms, NH (ICARTT)	0.2–0.6	100–4000	3723	543	0.180	0.182	0.009
36	Toronto, Canada	0.58	0–3500	4515	578	0.148	0.175	0.007
	Mean of All Studies (weighted equally)			$3034\overset{\times}{\div}2.57$	$379\overset{\times}{\div}1.51$	0.30 ± 0.15	0.136 ± 0.035	0.011 ± 0.005
	Mean of All Studies (weighted by area)			$1798\overset{\times}{\div}3.57$	$305\overset{\times}{\div}1.86$	0.38 ± 0.21	0.131 ± 0.035	0.014 ± 0.008
	Marine Mean Values			$207\overset{\times}{\div}3.72$	$58\overset{\times}{\div}1.81$	0.56 ± 0.18	0.152 ± 0.071	0.024 ± 0.014
	Continental Mean Values			$2444\overset{\times}{\div}2.90$	$403\overset{\times}{\div}1.67$	0.29 ± 0.19	0.115 ± 0.055	0.010 ± 0.008
	Global Mean Values			$502\overset{\times}{\div}5.52$	$116\overset{\times}{\div}2.97$	0.46 ± 0.22	0.139 ± 0.068	0.019 ± 0.014

ACPD
12, 20483–20517, 2012

Table 4. Percent overprediction of CCN concentration $\left(\frac{\Delta N_{CCN}}{N_{CCN}}\right)$ and simulated cloud droplet concentration $\left(\frac{\Delta N_d}{N_d}\right)$ averaged over the field studies' domain, with equal weighting given to each study location regardless of area. Reported are the mean ± one standard deviation across the 36 different data sets. Since individual field studies do not apply all scenarios, the overprediction values cannot be directly compared; however, the domain-averaged sensitivity ratios $\left(\frac{\Delta N_d}{\Delta N_{CCN}}\right)\left(\frac{N_{CCN}}{N_d}\right)$ are directly comparable, analagous to the sensitivities in Table 3.

Closure Scenario	N	Measured Mean N_{CCN} Overprediction (%)	Simulated Mean N_d Overprediction (%)	$\left(\frac{\Delta N_d}{\Delta N_{CCN}}\right)\left(\frac{N_{CCN}}{N_d}\right)$
$(NH_4)_2SO_4$	16	59 ± 64	18 ± 22	0.31 ± 0.16
Internal Mixture, Soluble Organics (κ_{org} = 0.11)	25	64 ± 118	21 ± 46	0.32 ± 0.16
Internal Mixture, Insoluble Organics (κ_{org} = 0)	25	37 ± 97	12 ± 36	0.33 ± 0.15
Size-Resolved, Internal Mixture, Insoluble Organics (κ_{org} = 0)	11	4 ± 15	1 ± 5	0.29 ± 0.12
External Mixture, Soluble Organics (κ_{org} = 0.11)	17	71 ± 115	23 ± 43	0.37 ± 0.15
External Mixture, Insoluble Organics (κ_{org} = 0)	16	16 ± 104	7 ± 42	0.33 ± 0.14

ACPD
12, 20483–20517, 2012

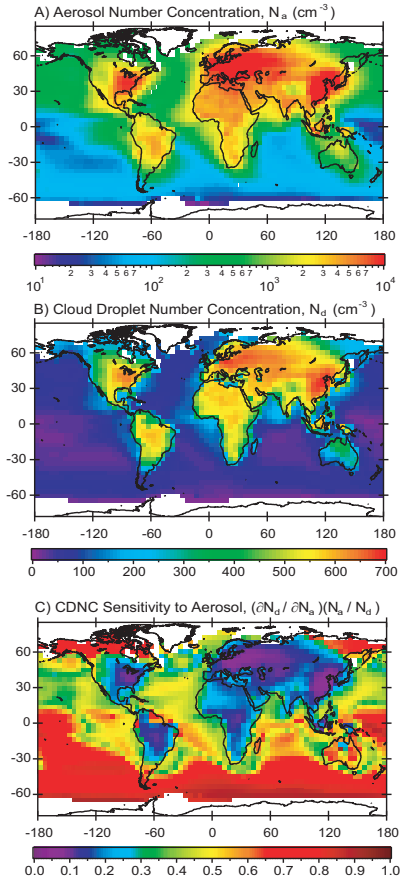

Fig. 1. Simulated global spatial distribution of the annual mean N_a **(A)**, N_d **(B)** and normalized sensitivity of N_d to N_a **(C)**.

ACPD
12, 20483–20517, 2012

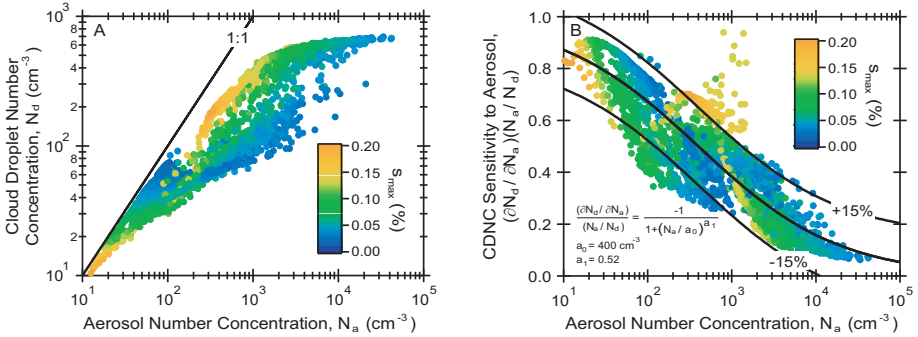

Fig. 2. Simulated N_d (left) and sensitivity of N_d to N_a (right) plotted versus simulated N_a for all grid model grid cells. Points are colored by the grid-cell s_{max}.

ACPD
12, 20483–20517, 2012

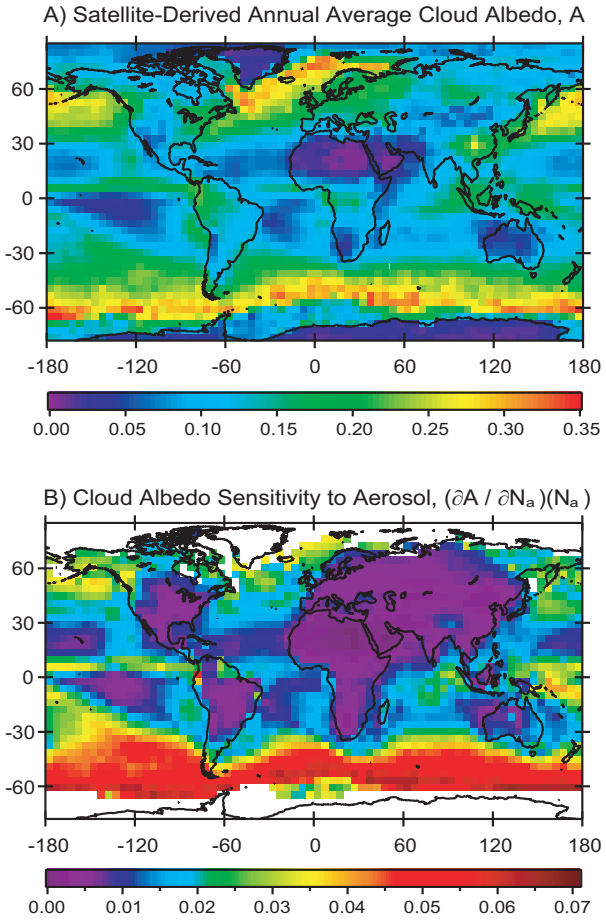

Fig. 3. Global spatial distribution of the annual mean A obtained from the NASA CERES satellite for 2003 **(A)**, and the derived semi-normalized sensitivity of A to N_a **(B)**.

ACPD
12, 20483–20517, 2012

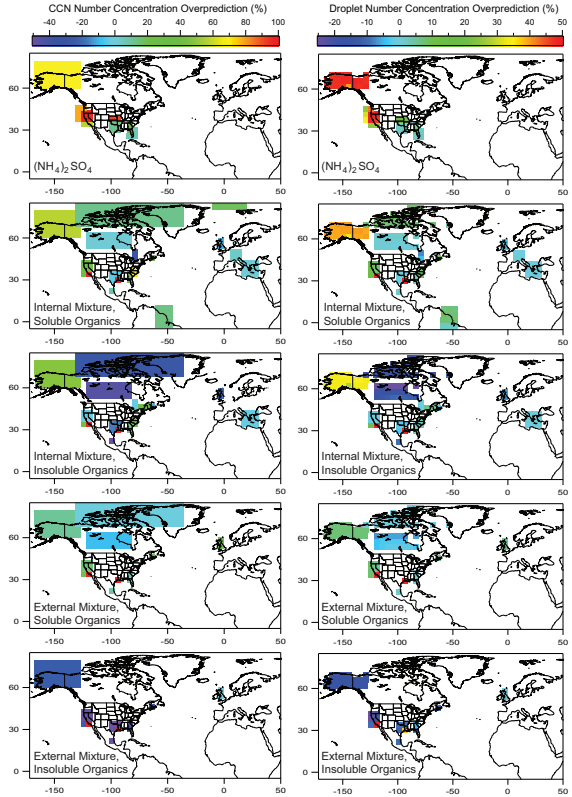

Fig. 4. Regional spatial distribution of measured N_{CCN} uncertainties derived from the closure studies (left) and the N_d uncertainty found by multiplying the measured $\frac{\Delta N_{CCN}}{N_{CCN}}$ by the simulated $\left(\frac{\partial N_d}{\partial N_a}\right)\left(\frac{N_a}{N_d}\right)$ (right).

ACPD
12, 20483–20517, 2012